The inexorable resistance of inertia determines the initial regime of drop coalescence

Joseph D. Paulsen[a,1], Justin C. Burton[a], Sidney R. Nagel[a], Santosh Appathurai[b,2], Michael T. Harris[b], and Osman A. Basaran[b]

[a]James Franck Institute and Department of Physics, University of Chicago, Chicago, IL 60637; and [b]School of Chemical Engineering, Purdue University, West Lafayette, IN 47907

Edited by William R. Schowalter, Princeton University, Princeton, NJ, and approved February 28, 2012 (received for review December 19, 2011)

Drop coalescence is central to diverse processes involving dispersions of drops in industrial, engineering, and scientific realms. During coalescence, two drops first touch and then merge as the liquid neck connecting them grows from initially microscopic scales to a size comparable to the drop diameters. The curvature of the interface is infinite at the point where the drops first make contact, and the flows that ensue as the two drops coalesce are intimately coupled to this singularity in the dynamics. Conventionally, this process has been thought to have just two dynamical regimes: a viscous and an inertial regime with a cross-over region between them. We use experiments and simulations to reveal that a third regime, one that describes the initial dynamics of coalescence for all drop viscosities, has been missed. An argument based on force balance allows the construction of a new coalescence phase diagram.

emulsions | fluid singularity

The collision and coalescence of water drops, so essential to raindrop growth and the development of thunderstorms, have captivated the attention of the atmospheric science community since the early studies by Benjamin Franklin and Lord Rayleigh (1). Coalescence also plays a central role in industrial processes involving emulsions or dispersions (2, 3). For example, in the petroleum industry, coalescence occurs during dispersed water removal and during oil desalting (4). It is a dominant process in determining the shelf life of emulsion-based products such as salad dressing and mayonnaise (5), and it occurs in dense spray systems and combustion (6). Also, sintering of two spherical particles closely resembles the coalescence of two dispersion drops in an emulsion (7). Moreover, the controlled coalescence of drops in microfluidic devices promises a host of potential applications in chemistry, biochemistry, and materials science (8).

The initial dynamics of coalescence are expected to be universal. The expansion of the liquid neck connecting two drops is controlled by the Laplace pressure, which diverges when the curvature of the liquid interface is infinite at the point where the drops first touch. Thus the change in topology, as two drops become one, is inextricably linked to a singularity in the dynamics. Different regimes of coalescence have been studied (9–25). The understanding that has emerged is that coalescence has just two dynamical regimes with a cross-over region between them: a viscous regime, which always dominates at sufficiently early times when the neck radius is microscopically small, and an inertial regime that occurs at late times if viscous effects become negligible. We use experiments and simulations to show that a third regime, one that describes the true initial dynamics of coalescence, has been missed. We present our results in terms of a phase diagram of coalescence that shows the three distinct dynamical regimes.

Results and Discussion

In the experiment, two pendant drops with radii $A \approx 0.1$ cm are suspended as in Fig. 1*A* from nozzles and slowly translated until they touch at their equators. Except where otherwise stated, the drops are silicone oil (surface tension $\gamma = 20$ dyn/cm and density $\rho = 0.97$ g/cm^3). The liquid viscosity, μ, or equivalently the dimensionless Ohnesorge number, $Oh = \mu/\sqrt{\rho\gamma A}$, is varied. We use a high-speed camera and electrical resistance measurements (24) to capture the dynamics.

In the simulations, two isolated spherical drops of radius A are connected by a small neck of radius $r_{\min} = 0.001A$. The dynamics that ensue are determined by solving the full Navier–Stokes equations by a finite-element algorithm that we have previously used successfully to study diverse situations involving drop breakup (26, 27). Creeping-flow simulations, where inertia is neglected, are also performed.

Fig. 1*A* shows two drops at the instant of contact, $\tau = 0$. To distinguish local versus global motion during merging, we subtract an image taken after the neck has grown to a small size from the one at $\tau = 0$ as shown in Fig. 1 *B* and *C* for fluid viscosities $\mu = 58{,}000$ cP ($Oh = 440$) and 49 cP ($Oh = 0.32$), respectively. At high viscosity, the two drops move together rigidly whereas at lower viscosity, the only appreciable motion occurs near the widening neck. This qualitative difference heralds the existence of a different and distinct regime.

The transition between these regimes can be understood from a force-balance argument that is based on the observation that in the perfectly viscous (i.e., Stokes) regime, the drops outside the immediate vicinity of the neck are rigidly translated towards each other. This was shown by Hopper (9, 10) in an exact analytic solution of coalescence in two dimensions (2D); this global motion was also seen in 3D Stokes simulations (11) and the early-time asymptotic behavior was later analytically extended to three dimensions (3D) (12). To be in the Stokes regime, therefore, the force of the neck pulling the two drops together must be sufficiently large to produce the required center-of-mass acceleration of each drop (i.e., the fluid on each side of the $z = 0$ plane). The asymptotic acceleration (9) is $a_{c.o.m.} = \gamma^2[\ln(r_{\min}/8A)]^2/2\pi^2\mu^2A$.

The coalescence is driven by surface tension. Therefore, an upper bound for the inward force of the neck on the drops is given by the surface-tension force, F_γ, around the circumference of the neck at its minimum radius. In 3D: $F_\gamma = 2\pi\gamma r_{\min}$. If F_γ is too small to translate the drops, each having a mass $m = \frac{4}{3}\pi A^3\rho$, the flows cannot be in the Stokes regime. Therefore, the Stokes regime can only be achieved when $F_\gamma \gtrsim ma_{c.o.m.}$ leading to the threshold criterion for entering the Stokes regime:

$$Oh \propto \left|\ln\left(\frac{1}{8}\frac{r_{\min}}{A}\right)\right|\left(\frac{r_{\min}}{A}\right)^{-1/2}. \quad [1]$$

Author contributions: J.D.P., J.C.B., S.R.N., S.A., M.T.H., and O.A.B. designed research; J.D.P. and S.A. performed research; J.D.P., J.C.B., and S.R.N. conducted the experiments; S.A., M.T.H., and O.A.B. conducted the simulations; J.D.P., J.C.B., S.R.N., S.A., M.T.H., and O.A.B. analyzed data; and J.D.P., J.C.B., S.R.N., S.A., M.T.H., and O.A.B. wrote the paper.

The authors declare no conflict of interest.

This article is a PNAS Direct Submission.

[1]To whom correspondence regarding experiments should be addressed. E-mail: paulsenj@uchicago.edu.

[2]To whom correspondence regarding simulations should be addressed. E-mail: santosha@purdue.edu.

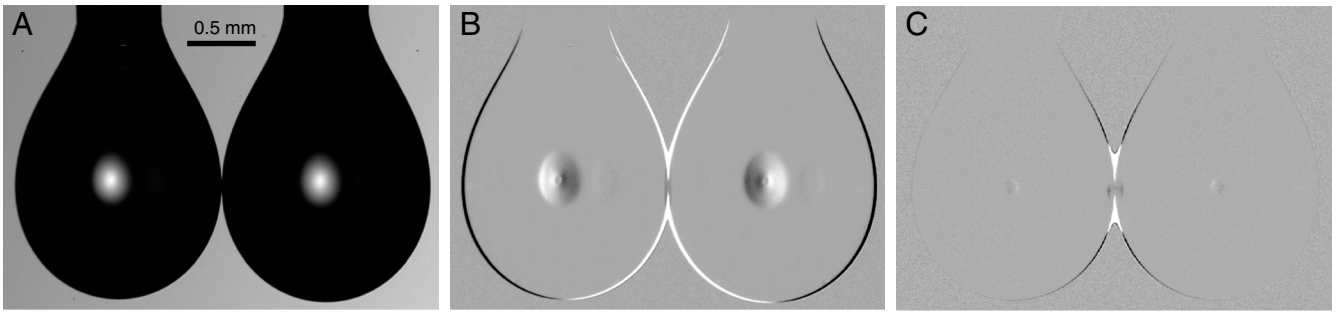

Fig. 1. Coalescence of silicone-oil drops with viscosities $\mu = 58{,}000$ cP ($Oh = 440$) and 49 cP ($Oh = 0.32$). (*A*) Two pendant drops at the instant they contact, $\tau = 0$. (The two bright spots are from back lighting.) We subtract an image taken after the neck has grown to a size $r_{min} = 0.25A$ from the one at $\tau = 0$ for *B*, $\mu = 58{,}000$ cP and *C*, 49 cP.

Therefore, for 3D drops of finite viscosity, the asymptotic dynamics, in the limit $r_{min}/A \to 0$, can never be in the Stokes regime. Below this threshold, F_γ is balanced by the inertia of the drops, $ma_{c.o.m.}$, and the dynamics are governed by local flows.

An analogous argument in 2D (where $F_\gamma = 2\gamma$ independent of r_{min}, and $m = \pi A^2 \rho$) suggests a phase boundary for 2D drops: $Oh \propto |\ln(r_{min}/8A)|/\sqrt{4\pi}$. Thus the logarithmic divergence of $a_{c.o.m.}$ also precludes the Stokes regime in 2D until r_{min}/A grows to a sufficient size.

Fig. 2*A* presents a phase diagram of the coalescence regimes for 3D drops, which includes the inertial and Stokes regimes in addition to this "inertially limited viscous" regime. In this regime, inertia and viscosity play a role in the dynamics; the inertia associated with each drop moving as a rigid object precludes the system from being in the Stokes regime. The inertially limited viscous to inertial cross-over was previously determined (24) to be $r_{min}/A \propto Oh$, in contrast to earlier work that had suggested that this cross-over occurs at $r_{min}/A \propto Oh^2$ (12, 17, 18). (Previously, there were believed to be only two coalescence regimes—a viscous one and an inertial one—so this cross-over is referred to as the viscous-to-inertial cross-over in the literature.) The inertially limited viscous to Stokes transition is described by **1**. We emphasize that, contrary to earlier studies, we find the Stokes and inertial regimes do not share a phase boundary; they are both preceded by the inertially limited viscous regime. Thus, at early times, a model of pure Stokes flow for the coalescence of spheres is never valid. We note that this is reminiscent of the singularity in drop breakup (28), where there are also three regimes, and the Stokes regime does not extend to $r_{min} \to 0$.

Having argued for the distinct identities of the inertially limited viscous regime versus the Stokes regime on theoretical grounds, we now offer evidence from experiment and simulation that these regimes are, in fact, different. First, we probe the global motion of the drops by measuring the velocity of the back of one drop, $v_{b.o.d.}$. Since this point is the farthest from the singularity, it isolates the global motion from the flow near the growing neck.

For 3D drops in the inertially limited viscous regime, force balance gives $a_{c.o.m.} \approx F_\gamma/m = 3\gamma r_{min}/2A^3\rho$. Using $r_{min} = \tau\gamma/\mu$ as seen in Fig. 3*E* consistent with previous experiments (17, 18, 20, 24, 25), we integrate to get

$$v_{b.o.d.} \approx \frac{3\gamma^2}{4\mu A^3 \rho}\tau^2 = \frac{3\mu}{4A^3\rho} r_{min}^2. \qquad [2]$$

If $Oh > 1$, then the flows eventually enter the Stokes regime, where to first order

$$v_{b.o.d.} \approx \frac{\gamma}{2\pi\mu A} r_{min} \left| \ln\left(\frac{1}{8}\frac{r_{min}}{A}\right)\right|. \qquad [3]$$

We find that the creeping-flow simulation follows the exact analytic 2D Stokes solution (**3**). In Fig. 2*B*, we plot $v_{b.o.d.}$ for drops of finite viscosity in the simulation and experiment. The curves exhibit the predicted superlinear growth of $v_{b.o.d.}$ at early times until the velocities merge onto the Stokes curve. The data show exceptional agreement between simulation and experiment.

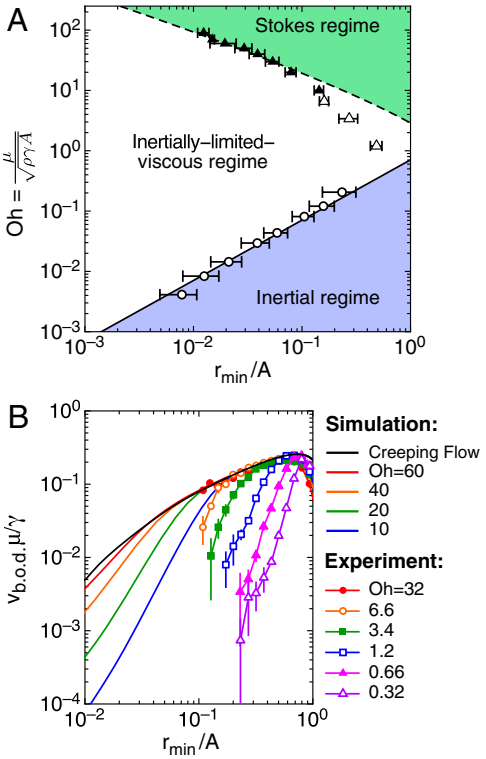

Fig. 2. Phase diagram for 3D coalescence. (*A*) While the inertial regime (12–24) and the Stokes regime (9, 10, 11, 12, 16) have been established in recent years, the inertially limited viscous regime is identified by this work. The inertially limited viscous to inertial cross-over was recently determined by experiments (open circles) and a scaling argument (solid line) (24). Here, we identify the inertially limited viscous to Stokes cross-over with a force-balance argument (dashed line: **1** with a proportionality constant of 1.4), simulations (filled triangles), and experiments (open triangles). The data depart from the prediction at large r_{min}, where we expect finite size effects to enter. (*B*) To observe the inertially limited viscous to Stokes cross-over, we measure $v_{b.o.d.}$ versus r_{min}/A over a range of viscosities from simulation (solid lines) and experiment (symbols). The velocities fall onto the creeping-flow curve at large r_{min}/A but peel away at smaller r_{min}/A. The velocity scaling at small r_{min}/A is qualitatively captured by **2**. The cross-over neck radius at which the macroscopic drop velocity $v_{b.o.d.}$ merges onto the Stokes solution is plotted in *A*, for the viscosities that exhibit such a cross-over within our range of data.

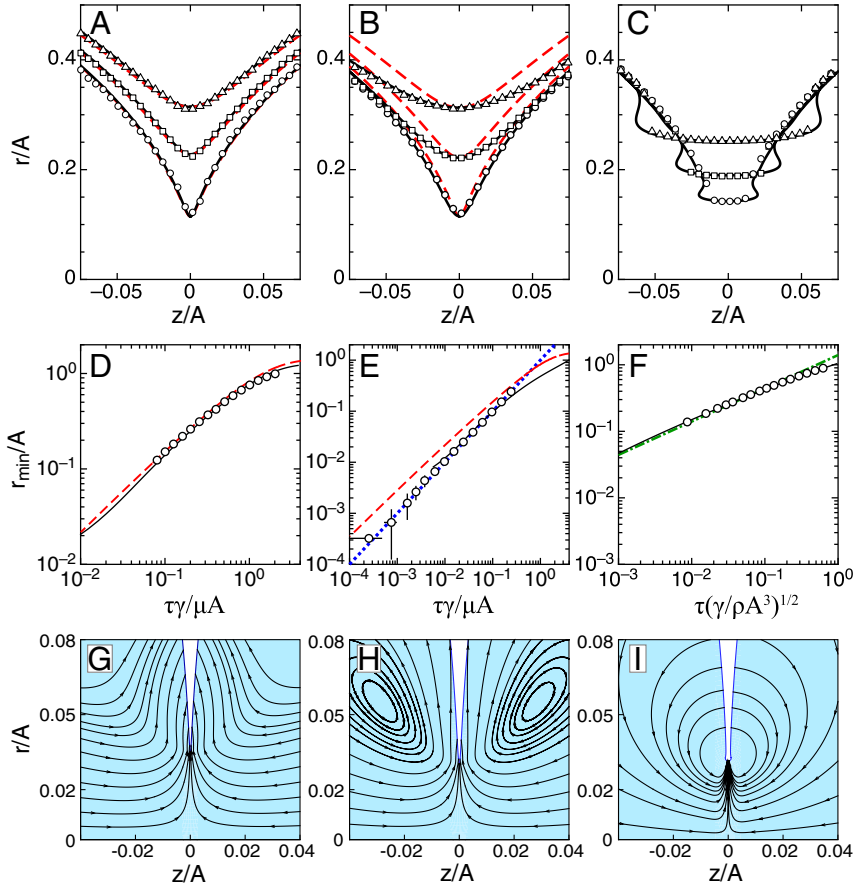

Fig. 3. Coalescence dynamics in the Stokes regime (*Left*: creeping-flow simulation, $Oh = 440$ experiment) versus the inertially limited viscous regime (*Center*: $Oh = 0.6$ simulation and experiment) and the inertial regime (*Right*: $Oh = 0.007$ simulation and experiment). (*A*,*B*,*C*) Neck profiles from simulation (solid lines) and experiment (symbols) at three different times, compared with the 2D Stokes theory in *A* and *B* [dashed lines (9)]. The Stokes profiles agree with high-viscosity data (*A*) but do not capture the broader interfacial shapes at $Oh = 0.6$ (*B*). (*D*,*E*,*F*) r_{min}/A versus rescaled time in the simulation (solid lines) and experiment (circles). High-viscosity drops (*D*) follow with the Stokes theory (dashed line). At intermediate viscosity (*E*), r_{min}/A does not agree with the Stokes theory but instead grows at the viscous-capillary velocity, $r_{min} = \tau\gamma/\mu$ (dotted line). At low viscosity in the inertial regime (*F*), $r_{min}/A = 1.4\tau^{1/2}(\gamma/\rho A^3)^{1/4}$ (dash-dot line). Note that in *E*, we begin plotting the simulation data at $\tau\gamma/\mu A = 6 \times 10^{-3}$, where we estimate that transients from the initial conditions have decayed. The experimental data in *E* were obtained by a high-speed electrical method on glycerol-salt-water drops ($\mu = 230$ cP, $\gamma = 65$ dyn/cm, $\rho = 1.2$ g/cm^3, and $A = 0.2$ cm) (24). (*G*,*H*,*I*) Instantaneous streamlines from simulations at $r_{min} = 0.03A$ in the (*G*) Stokes regime (creeping-flow simulation), (*H*) the inertially limited viscous regime ($Oh = 0.6$), and (*I*) the inertial regime ($Oh = 0.007$). The flows are qualitatively different in all three regimes.

We measure the cross-over neck radius at which the macroscopic drop velocity $v_{b.o.d.}$ merges onto the Stokes solution. We plot Oh versus r_{min}/A as the threshold for entering the Stokes regime on the phase diagram for 3D coalescence (Fig. 2*A*). At higher viscosities, the linear (Stokes) regime is entered at smaller r_{min}. The data agree well with the prediction from **1**.

The neck shapes also differ between the Stokes and the inertially limited viscous regimes. Because the exact analytic 2D solution extends over the entire domain of r_{min} (whereas the 3D solution only exists for small r_{min}), we use it here as a convenient way to account approximately for finite-size effects and to compare our experiment and simulation. In Fig. 3 *A* and *B*, we plot this 2D Stokes solution (9) in the neck region against experiment and simulation, for $Oh \gg 1$ and $Oh = 0.6$, in the *r*-*z* plane (with the origin at the initial point of contact). The Stokes solution agrees with the high-viscosity data, but it clearly fails to fit the shapes at $Oh = 0.6$ where both experiment and simulation show a much broader neck. In particular, the 2D analytic Stokes solution has a maximum neck curvature, κ, that obeys $1/\kappa A = \frac{1}{4}(r_{min}/A)^3$ to first order, which we find is in good agreement with our data in the Stokes regime (i.e., $Oh \gg 1$). In the inertially limited viscous regime (i.e., Oh approximately 1), we also find that $1/\kappa A$ scales as $(r_{min}/A)^3$ but with a significantly larger prefactor (approximately 1.2 instead of $\frac{1}{4}$).

The dynamics also differ between these two regimes. For high-viscosity drops, measurements of the neck radius r_{min} versus time in the experiment and simulation are consistent with the exact analytic 2D Stokes solution (Fig. 3*D*).* For lower-viscosity drops, the 2D Stokes solution does not fit the data (Fig. 3*E*). Instead, the neck radius grows linearly with time, consistent with $r_{min} = \tau\gamma/\mu$, a form that one might guess from dimensional analysis alone. (For the experimental data in Fig. 3*E*, we coalesce hemispherical drops attached to circular nozzles separated by a distance $2A$. This altered boundary condition does not affect our results: Using high-speed imaging, we find that for $r_{min} \ll A$, the dynamics are insensitive to this change in boundary conditions in both the inertially limited viscous and Stokes regimes.) This linear growth has been observed in previous experiments, but has incorrectly been assumed to be the dynamics of Stokes coalescence (17, 18, 20, 24, 25) and therefore was not recognized as evidence

*Previous viscous coalescence experiments (16, 17, 18, 24, 25) have compared the neck radius $r_{min}(\tau)$ against the theoretical prediction (12), $r_{min} \approx \tau\gamma|\ln(\tau\gamma/\mu A)|/\pi\mu$. This approximate form breaks down (12) for $r_{min} > 0.03A$. Therefore, we compare our measurements against the full analytic 2D solution (9), which can be done over the entire range of data.

PHYSICS

of a separate regime. We emphasize that the observed power law, $r_{min} \propto \tau$, is different from the inertial scaling where $r_{min} \propto \tau^{1/2}$ [as shown in Fig. 3*F* and by previous work (12, 13, 14, 15)], which demonstrates that the inertially limited viscous regime is distinct from the inertial regime as well.

Lastly, our simulations give the flow profiles near the singularity in the Stokes and the inertially limited viscous regimes (Fig. 3 *G* and *H*). The flow is expected to occur over a length scale comparable to r_{min} in the Stokes regime (12) and over a length scale r_{min}^2/A in the inertially limited viscous regime (24). Indeed, whereas features in the creeping-flow streamlines are roughly the size of r_{min}, the streamlines at intermediate *Oh* exhibit recirculation zones, which constrict the flows near the neck. Comparing the geometry of the streamlines further solidifies that the inertially limited viscous regime (Fig. 3 *B*,*E*, and *H*) is distinct from the one described by pure Stokes flow (Fig. 3 *A*,*D*, and *G*) and the one described by inertial flow (Fig. 3 *C*,*F*, and *I*). The streamlines in Fig. 3*I* corroborate the definition of the Reynolds number proposed in ref. 24 that dictates the inertially limited viscous to inertial cross-over.

Conclusion

As two drops begin to coalesce and a microscopic liquid neck forms between them, the curvature of the interface and the Laplace pressure that develops due to surface tension both diverge at the instant when the drops first touch. In drop coalescence with no external fluid, previous work (12) incorrectly led to the conclusion that only viscous forces, along with surface tension, should dominate on small scales, a dynamical regime referred to as the Stokes regime. Our work identifies a necessary condition for Stokes flow to occur. The dynamics cannot be in the Stokes regime until the surface-tension force around the neck is large enough to rigidly translate the two initially stationary drops towards each other. The inexorable resistance of inertia rears its head at even these small scales.

Therefore, a heretofore unknown dynamical regime controls the singularity at early times for drops of any viscosity. In this initial, asymptotic regime of drop coalescence in air, all of the underlying forces, that is inertial, viscous, and surface-tension forces, are important. Hence, the two dynamical regimes referred to as the Stokes regime, where inertia is negligible, and the inertial regime, where viscous force is negligible, can only be attained once the neck has grown to a sufficient size. Once the drop has entered the Stokes or inertial regimes, our measurements are consistent with the earlier predictions for the dynamics in those regimes.

A dynamically similar response is observed when a liquid filament breaks in air. At small neck size, the viscous and inertial regimes both give way to a third regime, where inertial, viscous, and surface-tension forces are all important (28). When a liquid filament breaks in another liquid, however, the dynamics are qualitatively different: In that case the asymptotic dynamics of thinning may occur in the absence of inertia (29, 30). Further insight may likewise be gained by studying drop coalescence inside a second immiscible liquid, which is a problem of immense practical importance (31, 32).

Materials and Methods

Experiment. High-speed imaging and electrical measurements were separately performed to capture the coalescence dynamics of isolated liquid drops in air. In high-speed imaging measurements, two silicone-oil drops with radii $A \approx 0.1$ cm were suspended side by side as in Fig. 1*A* from syringe needles. Different silicone oils were used to vary the liquid viscosity, μ, from 49 to 58,000 cP, while keeping other fluid parameters constant (surface tension, $\gamma = 20$ dyn/cm and density, $\rho = 0.96$ to 0.98 g/cm^3). Because they are highly wetting, pendant silicone-oil drops tend to climb up stainless steel syringe needles until the needles protrude from the bottoms of the drops. To prevent this, the needles were treated with an electronic coating (Novec EGC-1700, 3M) that inhibits wetting. The drops were aligned and then slowly translated with a micrometer stage until they gently touched at their equators. The resulting coalescence dynamics were recorded with a high-speed digital camera (Phantom v12, Vision Research).

The electrical method is described in detail in ref. 24. The experimental data in Fig. 3*E* were obtained by this method on glycerol-salt-water drops ($\mu = 230$ cP, $\gamma = 65$ dyn/cm, $\rho = 1.2$ g/cm^3, and $A = 0.2$ cm).

Simulation. The coalescence of two identical, isolated spherical drops of radius *A* of an incompressible Newtonian fluid that are surrounded by a dynamically passive gas is simulated by connecting them with a small bridge of radius r_{min} (typically equal to 0.1% of the drop radius) and height $z_{min} \ll r_{min}$. The ensuing coalescence dynamics are governed by the continuity and the Navier–Stokes equations, i.e., the Navier–Stokes system. Because the two drops are identical and the two-drop configuration is axially symmetric, the computational domain is the planar quadrant that consists of one of the drops and one-half of the bridge that is bounded by the plane of symmetry, the axis of symmetry, and the liquid–gas (L-G) interface. The Navier–Stokes system is solved subject to symmetry boundary conditions along the plane of symmetry and the axis of symmetry, and the kinematic and traction boundary conditions along the L-G interface (26, 27). This free boundary problem is solved numerically by a fully implicit method of lines arbitrary Lagrangian–Eulerian algorithm that uses the Galerkin/finite-element method (G/FEM) for spatial discretization and an adaptive finite difference method (FDM) for time integration (26, 27). On account of the free boundary nature of the problem, the interior of the flow domain is discretized by an adaptive elliptic mesh generation algorithm (33).

The G/FEM converts the transient system of nonlinear partial differential equations to a system of nonlinear ordinary differential equations (ODEs). The FDM time integrator reduces the system of ODEs to a large system of nonlinear algebraic equations. This system of equations is then solved by Newton's method with an analytically calculated Jacobian.

Starting from an initially quiescent state, the dynamics are followed until the two drops have coalesced into one and the dynamics have ceased. Simulations are carried out for both situations in which inertia is present, i.e., *Oh* is finite, and also when inertia is negligible, i.e, $1/Oh = 0$, such that the drops undergo creeping (Stokes) flow.

ACKNOWLEDGMENTS. We thank Michelle Driscoll, Efi Efrati, and Wendy Zhang. This work was supported by National Science Foundation (NSF) Grant DMR-1105145, the University of Chicago NSF Materials Research Science and Engineering Centers DMR-0820054, the NSF Engineering Research Center for Structured Organic Particulate Systems (EEC-0540855), and the Basic Energy Sciences Program of the US Department of Energy. Use of facilities of the Keck Initiative for Ultrafast Imaging is gratefully acknowledged.

1. Sartor JD (1969) Electricity and rain. *Phys Today* 22(8):45–51.
2. Evans DF, Wennerstrom H (1994) *The Colloidal Domain* (VCH Publishers, New York).
3. Saboni A, Gourdon C, Chesters A (1995) Drainage and rupture of partially mobile films during coalescence in liquid-liquid systems under a constant interaction force. *J Colloid Interface Sci* 175:27–35.
4. Eow JS, Ghadiri M (2002) Electrostatic enhancement of coalescence of water droplets in oil: a review of the technology. *Chem Eng J* 85:357–368.
5. Kumar S, Narsimhan G, Ramkrishna D (1996) Coalescence in creaming emulsions. Existence of a pure coalescence zone. *Ind Eng Chem Res* 35:3155–3162.
6. Ashgriz N, Poo JY (1990) Coalescence and separation in binary collisions of liquid drops. *J Fluid Mech* 221:183–204.
7. Djohari H, Martínez-Herrera JI, Derby JJ (2009) Transport mechanisms and densification during sintering: I. viscous flow versus vacancy diffusion. *Chem Eng Sci* 64:3799–3809.
8. Ahn K, Agresti J, Chong H, Marquez M, Weitz DA (2006) Electrocoalescence of drops synchronized by size-dependent flow in microfluidic channels. *Appl Phys Lett* 88:264105.
9. Hopper RW (1984) Coalescence of two equal cylinders: Exact results for creeping viscous plane flow driven by capillarity. *J Am Ceram Soc* 67:C262–C264.
10. Hopper RW (1990) Plane stokes flow driven by capillarity on a free surface. *J Fluid Mech* 213:349–375.
11. Martínez-Herrera JI, Derby JJ (1995) Viscous sintering of spherical particles via finite element analysis. *J Am Ceram Soc* 78:645–649.
12. Eggers J, Lister JR, Stone HA (1999) Coalescence of liquid drops. *J Fluid Mech* 401:293–310.
13. Menchaca-Rocha A, Martínez-Dávalos A, Núñez R, Popinet S, Zaleski S (2001) Coalescence of liquid drops by surface tension. *Phys Rev E* 63:046309.
14. Duchemin L, Eggers J, Josserand C (2003) Inviscid coalescence of drops. *J Fluid Mech* 487:167–178.
15. Wu M, Cubaud T, Ho CM (2004) Scaling law in liquid drop coalescence driven by surface tension. *Phys Fluids* 16:L51–L54.
16. Yao W, Maris HJ, Pennington P, Seidel GM (2005) Coalescence of viscous liquid drops. *Phys Rev E* 71:016309.

17. Thoroddsen ST, Takehara K, Etoh TG (2005) The coalescence speed of a pendent and a sessile drop. *J Fluid Mech* 527:85–114.
18. Aarts DGAL, Lekkerkerker HNW, Guo H, Wegdam GH, Bonn D (2005) Hydrodynamics of droplet coalescence. *Phys Rev Lett* 95:164503.
19. Lee T, Fischer PF (2006) Eliminating parasitic currents in the lattice boltzmann equation method for nonideal gases. *Phys Rev E* 74:046709.
20. Burton JC, Taborek P (2007) Role of dimensionality and axisymmetry in fluid pinch-off and coalescence. *Phys Rev Lett* 98:224502.
21. Fezzaa K, Wang Y (2008) Ultrafast x-ray phase-contrast imaging of the initial coalescence phase of two water droplets. *Phys Rev Lett* 100:104501.
22. Case SC, Nagel SR (2008) Coalescence in low-viscosity liquids. *Phys Rev Lett* 100:084503.
23. Case SC (2009) Coalescence of low-viscosity fluids in air. *Phys Rev E* 79:026307.
24. Paulsen JD, Burton JC, Nagel SR (2011) Viscous to inertial crossover in liquid drop coalescence. *Phys Rev Lett* 106:114501.
25. Yokota M, Okumura K (2011) Dimensional crossover in the coalescence dynamics of viscous drops confined in between two plates. *Proc Natl Acad Sci USA* 108:6395–6398.
26. Chen AU, Notz PK, Basaran OA (2002) Computational and experimental analysis of pinch-off and scaling. *Phys Rev Lett* 88:174501.
27. Suryo R, Basaran OA (2006) Local dynamics during pinch-off of liquid threads of power law fluids: Scaling analysis and self-similarity. *J Nonnewton Fluid Mech* 138:134–160.
28. Eggers J, Villermaux E (2008) Physics of liquid jets. *Rep Prog Phys* 71:036601.
29. Lister JR, Stone HA (1998) Capillary breakup of a viscous thread surrounded by another viscous fluid. *Phys Fluids* 10:2758–2764.
30. Cohen I, Brenner MP, Eggers J, Nagel SR (1999) Two fluid drop snap-off problem: Experiments and theory. *Phys Rev Lett* 83:1147–1150.
31. Dai B, Leal LG (2008) The mechanism of surfactant effects on drop coalescence. *Phys Fluids* 20:040802.
32. Cristini V, Bawzdziewicz J, Loewenberg M (2001) An adaptive mesh algorithm for evolving surfaces: Simulations of drop breakup and coalescence. *J Comput Phys* 168:445–463.
33. Christodoulou K, Scriven LE (1992) Discretization of free surface flows and other moving boundary problems. *J Comput Phys* 99:39–55.